Soils and Foundations 2012;52(5):830–841

The Japanese Geotechnical Society

Soils and Foundations

www.sciencedirect.com
journal homepage: www.elsevier.com/locate/sandf

Effect of earthquake ground motions on soil liquefaction

Shigeki Unjoh*, Masahiro Kaneko, Shojiro Kataoka, Kazuhiro Nagaya, Kazunari Matsuoka

Earthquake Disaster Prevention Division, Research Center for Disaster Management, National Institute for Land and Infrastructure Management, Ministry of Land, Infrastructure, Transport and Tourism, Asahi 1, Tsukuba 305-0804, Japan

Received 13 January 2012; received in revised form 12 September 2012; accepted 14 October 2012
Available online 1 December 2012

Abstract

During the 2011 off the Pacific Coast of Tohoku Earthquake, which was the largest earthquake in Japanese history, the soil liquefaction phenomenon was observed over a wide area along the Pacific Coast in Tohoku and in Kanto, including the Tokyo Bay area. Extensive damage was caused by the effect of soil liquefaction to residential lands and houses, as well as to infrastructures, such as roads, rivers, ports, and water supply/sewage systems. Since the 2011 off the Pacific Coast of Tohoku Earthquake occurred in a mega-size fault zone, with an area of 500 km × 200 km, the duration of the strong shaking was extremely long compared to that in the data recorded for past earthquakes. Clarifying the effect of the characteristics of the ground motion on the soil liquefaction mechanism is one of the essential studies to be conducted, and effective countermeasures for the damaged structures need to be found.

This paper presents the strong motion observation data obtained on the liquefied and the non-liquefied grounds and raises preliminary discussions on the mechanism of soil liquefaction based on this data. The effect of the duration and the number of cyclic loadings on the progress of the soil liquefaction phenomenon is also compared with that found in past strong motion data.

Keywords: 2011 off the Pacific Coast of Tohoku earthquake; Soil liquefaction; Ground motion; Strong motion observation; Duration time; Cyclic loading; Pore water pressure

1. Introduction

The 2011 off the Pacific Coast of Tohoku Earthquake, with a moment magnitude of M_w=9.0, occurred at 14:46 on March 11, 2011 [Japan Meteorological Agency (hereinafter referred to as JMA), 2011]. Destructive damage was caused by the strong shaking of the earthquake and by the tsunami, which followed it, along the Pacific Coast in Tohoku and Kanto, Japan. In particular, the huge tsunami, which arrived around 30 min after the main shock, hit the coastal areas of Aomori, Iwate, Miyagi, Fukushima, Ibaraki and Chiba Prefectures. A total of 19,272 people were killed or missing by the devastating earthquake (as of March 2012 by the Fire Defense Agency). Due to the extremely wide fault zone, numerous aftershocks occurred in sequence; 840 aftershocks with a magnitude of M_j=4.0 (M_j: JMA Magnitude) or greater were observed during the first 60 days after the main shock. The largest aftershock was M_j=7.6, which occurred off the coast of Ibaraki Prefecture, 29 min after the main shock. These aftershocks also significantly affected the progress of the damage and the delay in the recovery works.

Since 1997, the Ministry of Land, Infrastructure, Transport and Tourism (hereinafter referred to as MLIT) has administered the Seismograph Network, which consists of more than 700 stations with accelerometers equipped on

*Corresponding author.
E-mail address: unjoh-s92ta@nilim.go.jp (S. Unjoh).
Peer review under responsibility of The Japanese Geotechnical Society.

Production and hosting by Elsevier

0038-0806
http://dx.doi.org/10.1016/j.sandf.2012.11.006

the ground surface [National Institute for Land and Infrastructure Management (hereinafter referred to as NILIM (2012))]. The stations were set at intervals of 20–40 km along rivers and national highways administered by MLIT. The observed data (PGA, Spectrum Intensities (SI-values) and JMA Instrumental Seismic Intensities) are immediately sent to the Tsukuba office of NILIM when an earthquake of a certain intensity or greater occurs, and the data is open to the public via the NILIM website. During the 2011 off the Pacific Coast of Tohoku Earthquake, strong motion data were obtained at about 400 MLIT stations.

During the 2011 off the Pacific Coast of Tohoku Earthquake, soil liquefaction caused extensive damage to residential lands and houses, as well as to infrastructures, such as roads, rivers, ports, and water supply/sewage systems, over a wide area along the Pacific Coast in Tohoku and in Kanto, including the Tokyo Bay area (MLIT Committee to Study Countermeasures against Soil Liquefaction, 2011). Due to the large fault zone, the duration of the strong shaking was extremely long.

This paper presents the strong motion observation data obtained on the liquefied and the non-liquefied grounds and raises preliminary discussions on the mechanism of soil liquefaction based on this strong motion observation data. The effect of the duration and the number of cyclic loadings on the progress of the soil liquefaction phenomenon is also compared with that found in past strong motion data.

2. Strong motion observation data obtained at MLIT seismograph network (NILIM, 2012)

Fig. 1 shows the observed data (PGA, Spectrum Intensities (SI-values) and JMA Instrumental Seismic Intensities) of the MLIT Seismograph Network during the 2011 off the Pacific

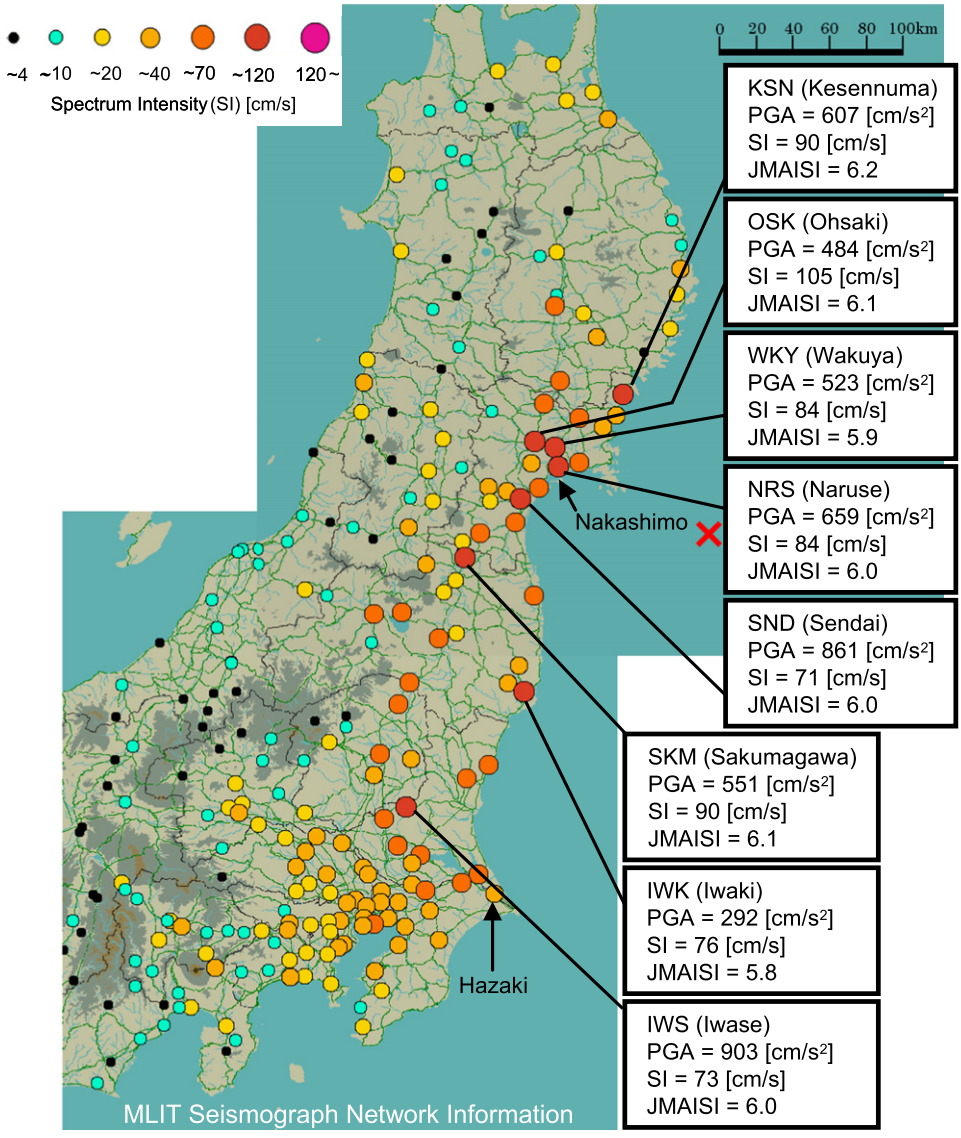

Fig. 1. Map of SI-values observed by MLIT Seismograph Network. (PGA, SI and JMA instrumental seismic intensities are shown for the sites where SI was 70 cm/s or larger. PGA and SI are calculated by synthesizing two horizontal components.).

Coast of Tohoku Earthquake (Kataoka et al., 2011). In order to estimate the vulnerability of the damage in the affected area, isoseismal maps are also produced for PGA, SI-values and JMA instrumental seismic intensities by the interpolation of the strong motion records. Fig. 2 presents a PGA map in which the data obtained by MLIT, JMA and the National Institute for Earth Science and Disaster Prevention (hereinafter referred to as NIED) are all included (NIED, 2012). It is clearly recognized that the strong shaking (for example, PGA > 250 [cm/s^2]) was observed over a wide area.

Fig. 3 shows typical time histories for the ground acceleration observed at KSN, OSK and IWS Stations of the MLIT Seismograph Network shown in Fig. 1. Two major wave groups, observed in the KSN and OSK records, correspond to the first two ruptures, which occurred near the epicenter, while the peak acceleration, observed at IWS, corresponds to the third rupture, which occurred about 200 km south of the

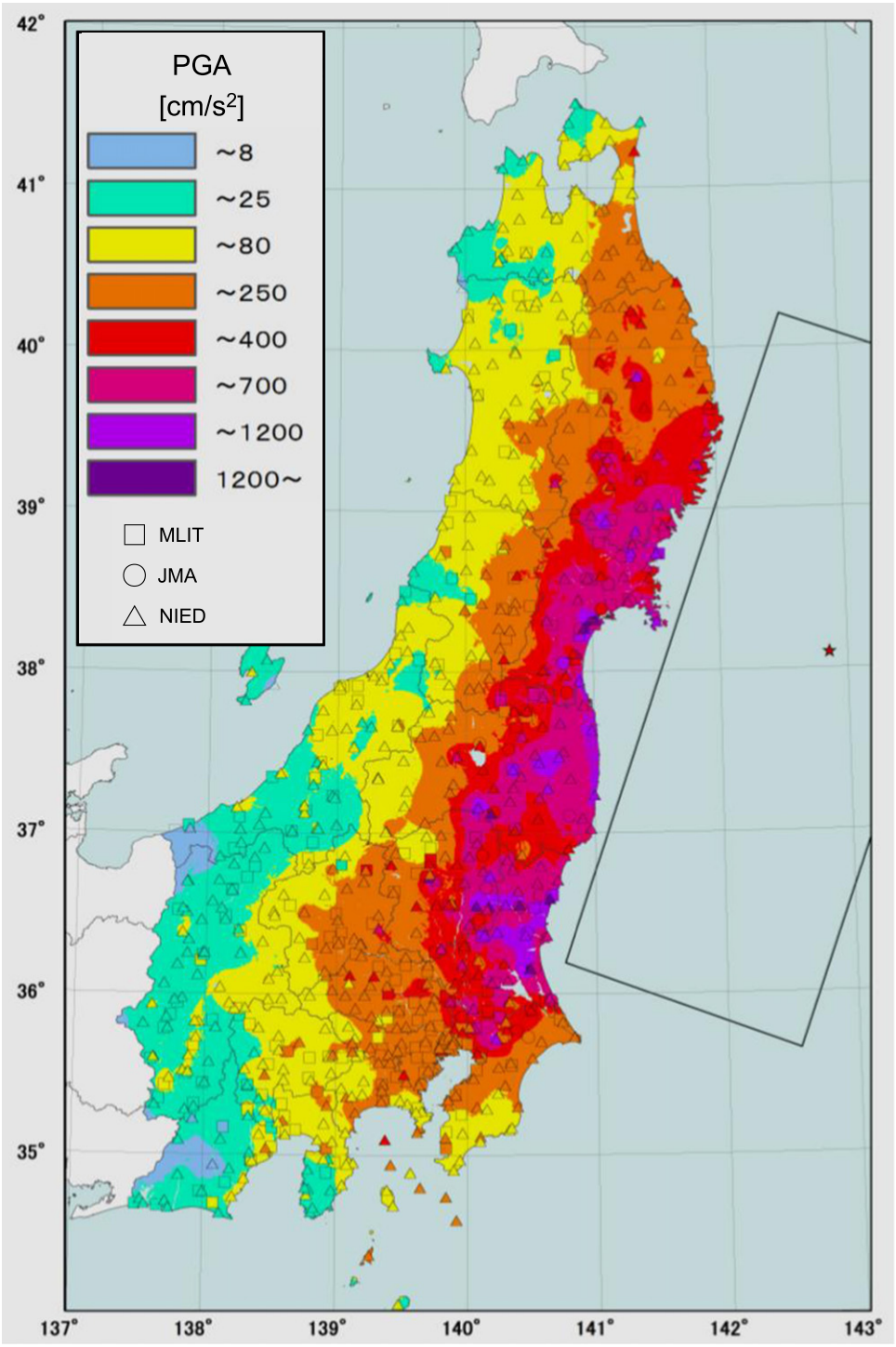

Fig. 2. Estimated PGA map obtained from the observation data.

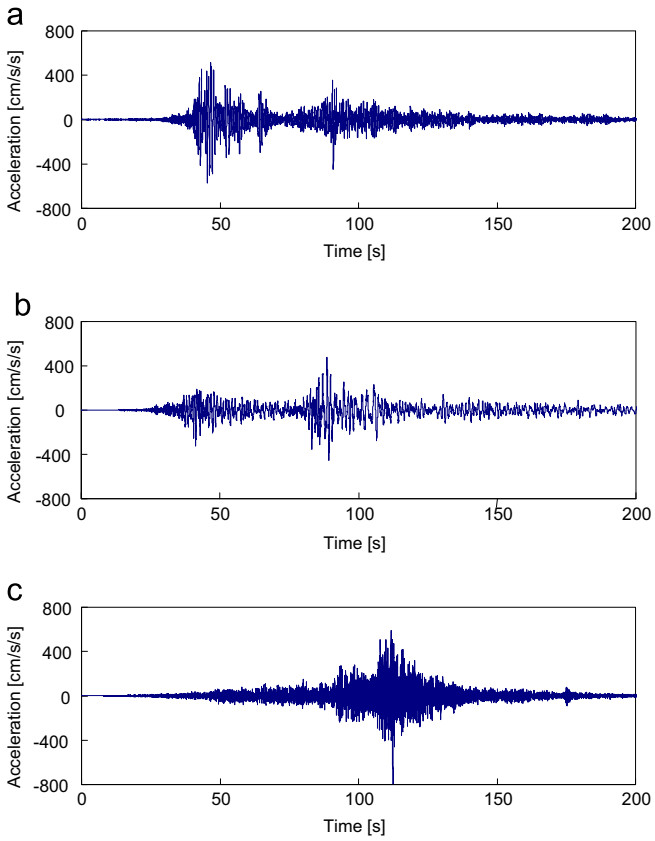

Fig. 3. Ground acceleration time histories observed at KSN, OSK and IWS Stations. (a) KSN (EW component). (b) OSK (NS component). (c) IWS (NS component).

Photo 1. Data logger of KSN Station which was damaged by the tsunami.

epicenter (Yoshida et al., 2011). It should be noted here that the data logger of the KSN Station was installed on the second floor of a two-story building and that that building was hit by the tsunami, as shown in Photo 1, but the recorded data was successfully collected from the damaged building. Several stations in the coastal areas were washed away by the tsunami and their data were lost. The largest PGA was 903 cm/s^2 at IWS Station and the largest SI-value was 105 cm/s at OSK Station.

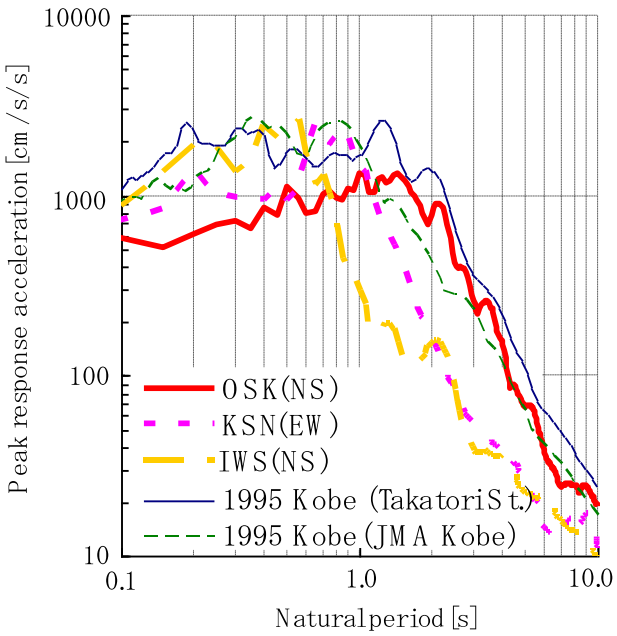

Fig. 4. Acceleration response spectra of the strong motions observed at OSK, KSN and IWS Stations compared with those at Takatori Station and the JMA Kobe Marine Observatory for the 1995 Kobe Earthquake.

Fig. 4 compares the acceleration response spectra of the ground motions shown in Fig. 3 with those observed at Takatori Station and the JMA Kobe Marine Observatory during the 1995 Kobe Earthquake. The two response spectra for the 1995 Kobe Earthquake are mostly larger than the other three over the natural period of 0.1–10 s. The response spectra for the two earthquakes, around 0.6–0.9 s, are almost equal, but those of the 2011 off the Pacific Coast of Tohoku Earthquake, around 1.0–2.0 s, which generally affects the damage of structures, including houses and bridges, is relatively smaller than those of the 1995 Kobe Earthquake. Only three selected pieces of strong motion data recorded during the 2011 earthquake are shown here, but it should be noted that the spectral strength level of the records, around 1.0–2.0 s, is comparable to the upper spectral level obtained from all the recorded ground motions. This may account for the difference in structural damage due to the ground motions between these two earthquakes.

3. Observed motions with effect of soil liquefaction

3.1. Typical time history of ground acceleration

Fig. 5 shows a time history of the ground acceleration observed at Hazaki Station in Chiba Prefecture. The NS component is shown. Photo 2 shows the sand boiling observed just 5 m from the observation station. A particular wave pattern, which is typically observed on a liquefied ground, was recognized. The acceleration amplitude suddenly decreased at the time of 95 s and the vibration period was elongated after that. Typical pinching motion with pulse-like amplitude is also observed in the acceleration waveform.

3.2. Observed motions at a levee

Time history records of ground acceleration and pore water pressure were obtained at a levee during the 2011 off the Pacific Coast of Tohoku Earthquake as well as during the 2003 Miyagi North Earthquake of July 26, 2003 (Kataoka et al., 2011). Fig. 6 shows the location of Nakashimo Station and the arrangement of the accelerometers and the piezometers in the levee on the right bank of the Naruse River in Miyagi Prefecture. Sensor arrays were installed at the bottom and near the crown of the levee. The bottom sensor was installed at a depth of about 13 m from the crown. The piezometers were installed in a sandy soil layer at a depth of about 9 m, which was evaluated as liquefiable soil during strong earthquakes. It should be noted here that the measurement range of the installed piezometers, for detecting pore water pressure, was assumed as 101.3 kPa (=1 atm), and that pressure data over 101.3 kPa was out of the range, which will be discussed later. The station was hit by the tsunami as shown in Photo 3; its inundation height was estimated to be about 1 m based on the trace of water surface on the inside wall of the instrument shed. Observed data from the sensor arrays at the berm, densified with the Sand Compaction Pile (SCP) method, were not obtained.

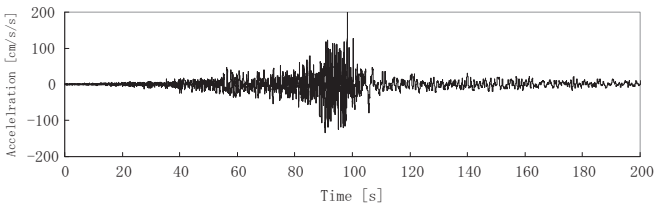

Fig. 5. Acceleration time history observed at Hazaki Observation Station, Chiba.

Photo 2. Sand boiling observed near Hazaki Observation Station.

Fig. 7 shows the time history records observed at Nakashimo Station during the main shock of the 2011 off the Pacific Coast of Tohoku Earthquake. The acceleration of the NS and EW components at the bottom and at the crown, and the excess pore water pressure in the sandy soil layer, are shown. The NS and EW components almost correspond to the longitudinal and transverse directions of the levee. The excess pore water pressure is shown as a non-dimensional pore water pressure ratio. It is defined as the ratio between the overloading stress and the pore water pressure; thus, ratio=1.0 means the overloading weight is fully supported by the pore water pressure that corresponds to full liquefaction. The overloading stress at the location of the piezometer, 119 kPa, was calculated from the soil boring data at this site.

Two major wave groups were observed, similar to the typical waveform found during this earthquake, and the

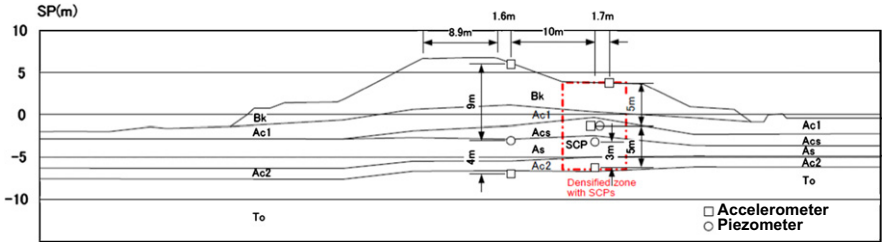

Fig. 6. Location of Nakashimo Station and arrangement of accelerometers and piezometers in a levee.

Photo 3. Nakashimo Station before (2008) and after (April 4, 2011) the earthquake (tsunami inundation height was about 1 m in this area).

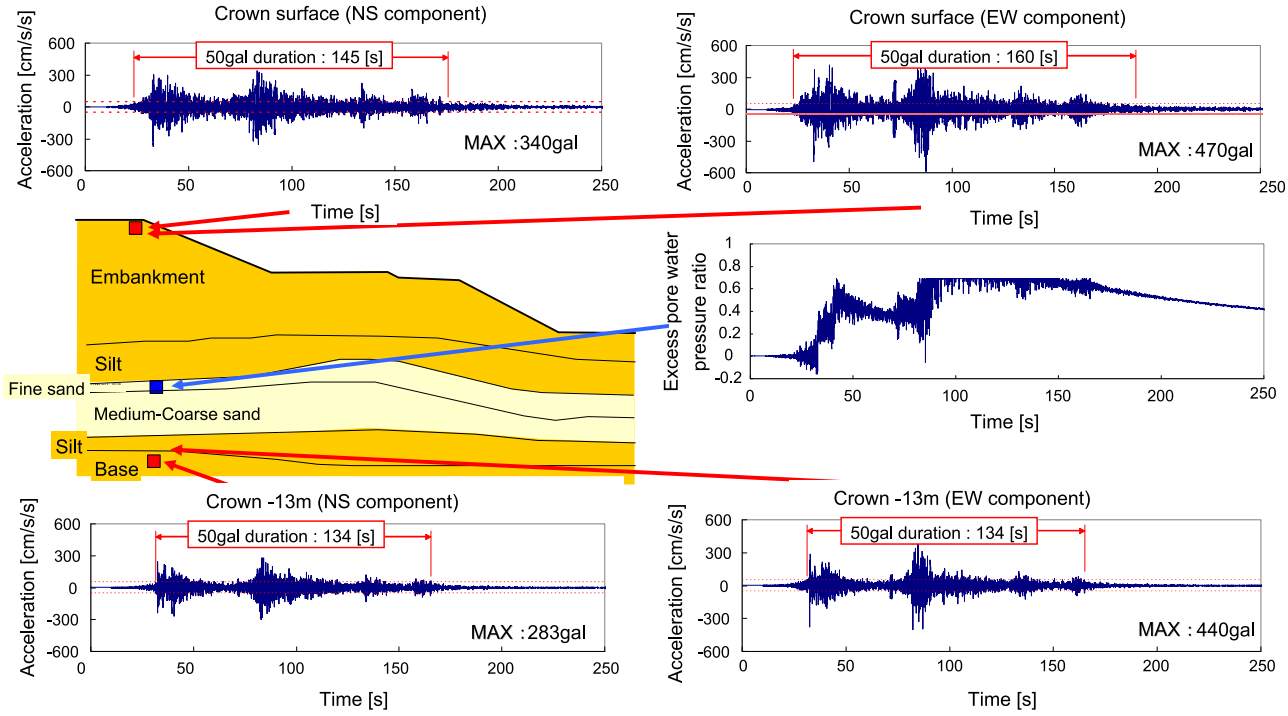

Fig. 7. Time history records observed at Nakashimo Station during the 2011 off the Pacific Coast of Tohoku Earthquake.

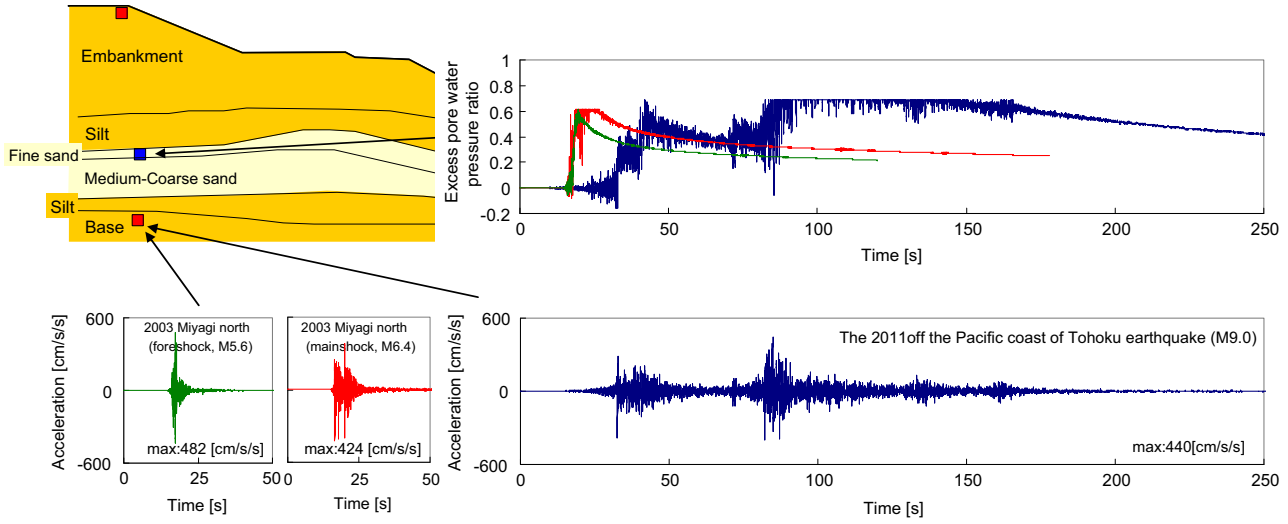

Fig. 8. Comparison of accelerations (EW Component) and excess pore water pressure observed at Nakashimo Station during the 2003 Miyagi North Earthquake and the 2011 off the Pacific Coast of Tohoku Earthquake.

duration of the strong shaking was extremely long, about 130–160 s, assuming that duration is defined as the time interval with the acceleration amplitude of 50 gal or greater. The peak acceleration at the bottom of the levee was 283 gal in the NS direction and 440 gal in the EW direction.

The excess pore water pressure rises with an increase in the acceleration amplitude, and falls with a decrease in the acceleration between the two major wave groups. Then it rises again with the increase in acceleration amplitude in the second wave group. In the first wave group, the excess pore water pressure ratio increases up to about 0.7 and gradually decreases; then the ratio increases again over 0.7. The pressure levels over 0.7 were not measured because of the range limitation of the piezometers used in this study, as discussed in the above. The duration, during which the ratio was greater than 0.7, was about 50 s; this is a relatively long time. It should be noted here that the liquefaction phenomenon, including the sliding/cracking of soil and sand boiling, was not clearly observed around the station. However, as discussed before, such damage could not be accurately confirmed since this area was hit by the tsunami.

Fig. 8 compares the time histories of the acceleration and the excess pore water pressure observed at Nakashimo

Station between the 2003 Miyagi North Earthquake and the 2011 off the Pacific Coast of Tohoku Earthquake. As for the 2003 Miyagi North Earthquake, two earthquakes with $M_j = 5.6$ and 6.4 occurred in sequence with an interval of about 7 h.

The 2003 earthquake was a shock-like earthquake during which the acceleration increased suddenly in a very short time and the duration was very short, about 5 s, while it was about 130–160 s during the 2011 earthquake. The peak acceleration at the bottom of the levee was almost the same for the two earthquakes, at 482 and 424 gal for the 2003 earthquake and 440 gal for the 2011 earthquake.

Increases in the excess pore water pressure showed a similar pattern to that of the acceleration. In the 2003 earthquake, the excess pore water pressure increased in a very short time and the duration, during which the ratio was greater than 0.6, was about 10 s. The excess pore water pressure decreased when the acceleration amplitude fell to less than a certain level. It was found that the tendency for the release of pressure seemed to be the same among the three records. It should be noted here that 7 h passed between the two 2003 earthquakes, and that the raised excess pore water pressure in the first earthquake was reduced completely to zero after 7 h at this site.

Fig. 9 shows a rough estimation of the release time of the excess pore water pressure at Nakashimo Station during the 2011 off the Pacific Coast of Tohoku Earthquake. About 800 s was the actual recorded time and the pressure ratio fell from 0.7 to 0.2. The relation between the excess pore water pressure ratio and the release time has been studied. Considering the consolidation mechanism, the relation is assumed in this study as

$$\Delta u(t) = C_1 \cdot \exp(C_2 \cdot t) \quad (1)$$

where

$\Delta u(t)$: Excess pore water pressure ratio
t: Time [s]
C_1, C_2: Coefficients

Coefficients C_1 and C_2 are determined from the observed time history data using the least squares approximation method. Since three aftershocks were recorded in the observed time history data, shown in Fig. 9, C_1 and C_2 are obtained for each time interval. The intervals are the same among (I) 170–360 s, (II) 360–500 s, (III) 500–720 s and (IV) 720–830 s. The average of the obtained C_2 for the four intervals becomes -0.002, and C_1 is obtained as 0.56 for the interval of (IV). Therefore, the equation to estimate the release time from the time of 720 s is derived as

$$\Delta u(t) = 0.56 \cdot \exp(-0.002 \cdot t) \quad (2)$$

Using Eq. (2), the time for the complete dissipation of pressure is estimated to be from 2000 to 3000 s.

Such a release time for the excess pore water pressure is dependent on the water permeability of the soil layer. Fig. 10 presents a grain size accumulation curve for the sandy soil layer (medium to coarse sand layer). Since the layer consists of relatively coarse sand, the permeability estimated by Creager's Method (Creager et al., 1945), 2.9×10^{-4} m/s, is relatively high as well. The releasing mechanism for the pore water pressure, on which on the duration of the shaking and the soil characteristics depend, is also one of the important issues that should be studied.

The mechanism to increase the pore water pressure with the ground motion characteristics is studied. Fig. 11 shows the relations between the time histories of the excess pore water pressure and the accumulated acceleration amplitudes for the 2003 and 2011 earthquakes. In this study, the acceleration waveforms in the EW direction, observed at the bottom of the levee, are employed for the calculation of the accumulated acceleration amplitudes; peak amplitudes with an acceleration of 200 gal or greater are picked up from the acceleration waveforms and totaled through time 0–t [s] to calculate the accumulated acceleration amplitudes at time t [s]. It is found that the excess pore water pressure increases in the short time of 5 s for the 2003 earthquake, while it increases gradually in a staircase pattern in about 30 s for the 2011 earthquake. It should be noted here that

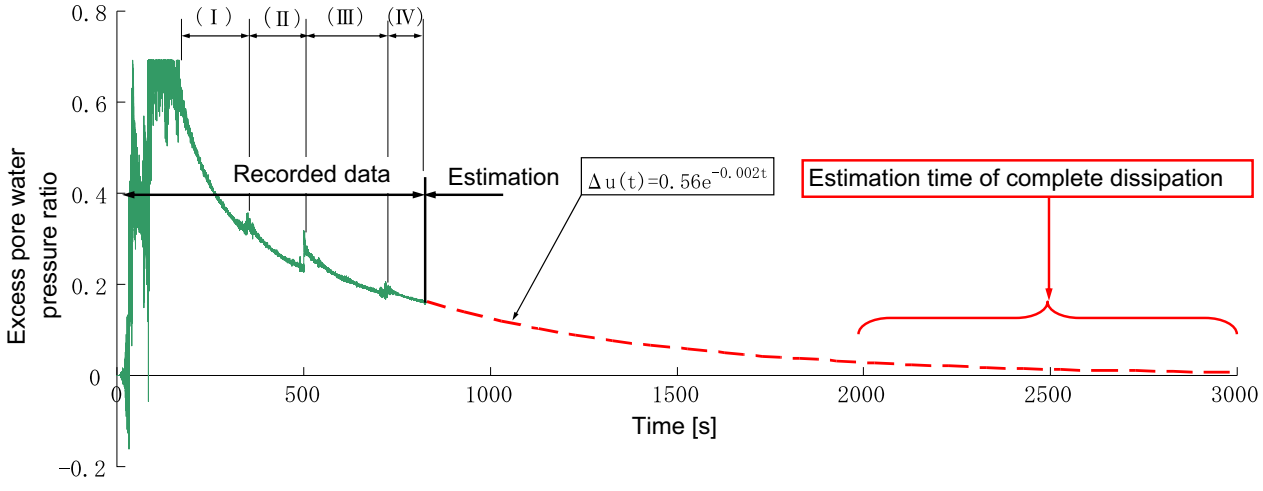

Fig. 9. Preliminary estimation of the release time of the excess pore water pressure at Nakashimo Station during the 2011 off the Pacific Coast of Tohoku Earthquake.

peak amplitudes of 200 gal or greater are assumed at the site, but how the large acceleration or the strain amplitude significantly affects the increase in excess pore water pressure is yet another research issue to be addressed.

A good agreement among the three records is commonly found for the relation between two parameters, as shown in Fig. 11, which means that the increase in excess pore water pressure is closely related to the accumulation of shaking, that is, the number of cycles and the amplitude.

The preliminary simulation analysis of the earthquake response of the Nakashimo levee was conducted using the observation data (Kataoka et al., 2011). A computer code for the 1-dimensional effective stress analysis method was employed (Yoshida and Towhata, 2003). The computer code, YUSAYUSA-2, was developed to simulate the earthquake response of the level ground taking account of the strain-dependent nonlinear characteristics, dilatancy and energy dissipation in the semi-infinite region. The material properties used in the simulation are summarized in Table 1. The cohesion is assumed as 0 for the sandy layers and estimated using the N-value for the cohesive layers. The internal friction is assumed as 0 for the cohesive layers and estimated using the N-value for the sandy layers. The rigidity is obtained based on PS logging. The porosity, the fine fraction, the volume compressibility and the phase transformation angle are based on the soil test results and the site conditions. The permeability is estimated by Creager's method using a 20% passing particle size, D_{20}. R_{L20} and R_{L5} are obtained based on the references of JRA (Japan Road Association): Bridge Design Specifications (1996) and Yoshida and Towhata (2003), respectively.

Fig. 12 shows the observed motion at the bottom layer, which was used as the input motion for the model, and the observed and the simulated motions at the crown. Although the short period component of the simulated motion is somewhat smaller than the observed one, the entire waveform was reproduced well. The observed and the simulated time histories of the excess pore water pressure are also compared in Fig. 12. The hydrodynamic pressure and the dissipation of the pore water pressure were not reproduced at all. In particular, the tendencies for pressure reduction were quite different between the observed and the analyzed motions. Since the excess pore water pressure beneath the embankment tended to be greater than elsewhere, the dissipation of excess pore water pressure in a lateral direction should be considered, although that in the vertical direction is taken into account in the simulation (Yoshida and Towhata, 2003). Further study is necessary using more precise soil characteristics, including the water permeability, by means of freezing soil sampling methods and 2-dimensional simulation models, to improve the agreement between the observed records and the analytical results.

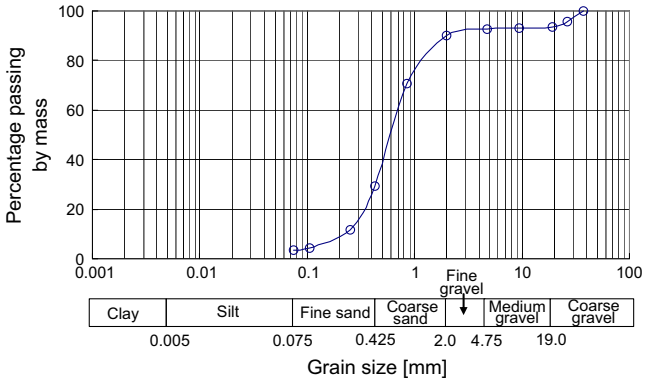

Fig. 10. Grain size accumulation curve of the sandy soil layer (medium to coarse sand) at Nakashimo Station.

3.3. Observed motions at reclaimed lands

Dense array strong motion observations have been made at Narashino Station in Chiba Prefecture, in the Tokyo Bay area (NILIM, 2012). Fig. 13 shows the locations of the sensors; eight locations in total have been measured since 1997. The southwest area under the blue dotted line is a reclaimed land area which was constructed in the mid-1970s. Earthquake ground motions both inland and in the reclaimed land were observed during the 2011 off the Pacific Coast of Tohoku Earthquake.

The depth of the reclaimed layer gradually increases toward the sea; it is about 10 m in depth along the coast line.

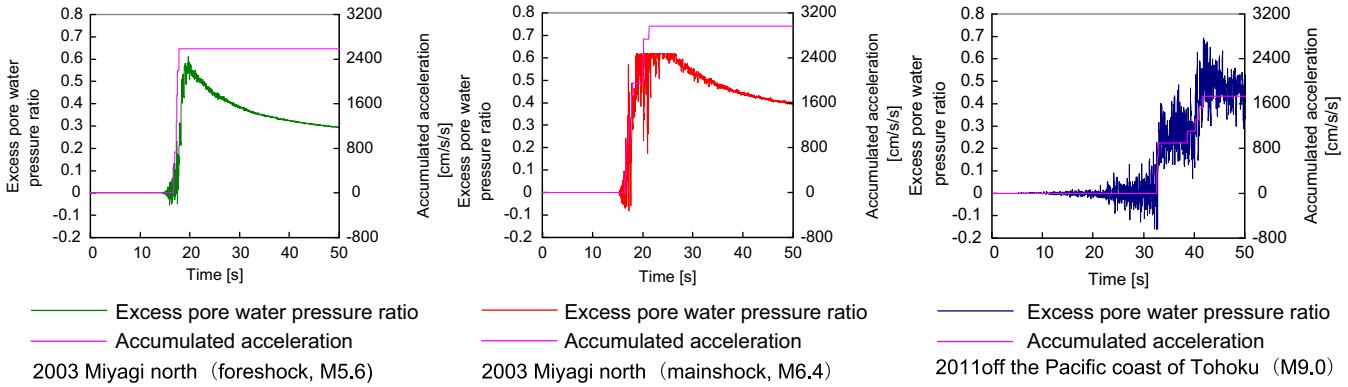

Fig. 11. Relations between accumulated acceleration and excess pore water pressure for the 2003 and 2011 earthquakes.

Table 1
Material properties set up for the 1-D effective stress analysis.

	Category	Upper depth (m)	Unit weight γ (kN/m^3)	Cohesion c (kN/m^2)	Ultimate shear strength τ_f (kN/m^2)	Internal friction ϕ (deg.)	Rigidity G_0 (kN/m^2)	Porosity n	Permeability k (m/s)	Fine fraction FC (%)	Volume compressibility m_v (m^2/kN)	Phase transformation angle	R_{L5}	R_{L20}
1	BK1	0.00	17	0.0	30.00	–	5.132E+04	0.44	4.344E−05					
2	BK1	1.00	17	0.0	30.00	–	5.132E+04	0.44	4.344E−05					
3	BK1	2.10	17	0.0	30.00	–	5.132E+04	0.44	1.006E−05					
4	BK1	3.20	17	0.0	30.00	–	5.132E+04	0.44	2.111E−05					
5	BK2	4.20	14	83.4	–	0	6.604E+04	0.69	3.370E−06					
6	BK2	5.20	14	83.4	–	0	6.604E+04	0.69	3.751E−10					
7	Ac1	6.30	14	54.0	–	0	4.732E+04	0.69	3.751E−10	76.2	–	–	–	–
8	Ac1	6.80	14	54.0	–	0	4.732E+04	0.69	3.751E−10	76.2	–	–	–	–
9	Ac1	7.80	14	54.0	–	0	4.732E+04	0.69	9.635E−10	86.8	–	–	–	–
10	Acs	8.87	17	0.0	19.08	–	3.256E+04	0.44	2.916E−04	3.6	3.250E−05	22.2	0.136	0.095
11	As1	9.00	17	0.0	33.01	–	4.496E+04	0.44	2.916E−04	3.6	3.289E−05	26.6	0.200	0.140
12	As1	10.00	17	0.0	34.87	–	05.496E+04	0.44	3.778E+04	4.5	3.379E−05	26.6	0.195	0.137
13	Ac2	11.45	14	127.5	–	0	9.072E+04	0.69	4.000E−10	88.6	–	–	–	–
14	To	12.20	20	–	–	–	2.764E+05	–	–	–	–	–	–	–

Note: BK: embankment, Ac: silt, Acs: fine sand, As: sand, To: base.

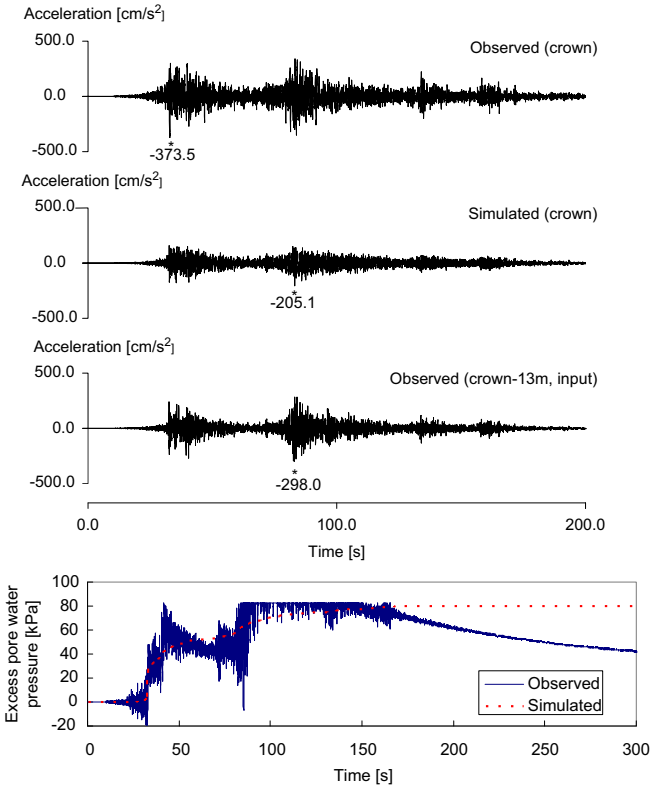

Fig. 12. Comparisons of the observed and analyzed acceleration and pore water pressure.

The standard *N*-value for the reclaimed layer is about 5–10. Under the reclaimed layer, there are relatively stiff Yurakucho and Shimousa base layers. The Yurakucho layer is a sandy layer formed in the Holocene epoch with an *N*-value of around 10; on the other hand, the Shimousa layer is a sandy layer formed in the Pleistocene epoch with an *N*-value greater than 20–30.

Extensive soil liquefaction and damage, including sand boiling, spouting water, settlement, cracking, sliding and lateral spreading were observed over the wide area of reclaimed land, while almost no soil liquefaction was found in the inland area. There is a canyon area along the river that is close to ST1, and some sand boiling was observed there, but the degree of liquefaction was remarkably smaller than that observed in the reclaimed land area.

Fig. 14 shows the acceleration time histories observed for the dense arrays and the damage around the stations. The EW components at the ground surface level (−2 m) are shown. Almost the same wave pattern is found in the time histories for the reclaimed and the inland areas. The peak accelerations are about 200–250 gal. It is not shown here, but the peak acceleration of about 100 gal was observed in the base layer with a relatively high *N*-value for both the reclaimed and the inland areas. The duration with an acceleration amplitude of 50 gal or greater is about 40–50 s. The elongation of the natural period of shaking is clearly found at the time of 80 s in the time histories of the reclaimed land area, and sand boiling and cracks are found

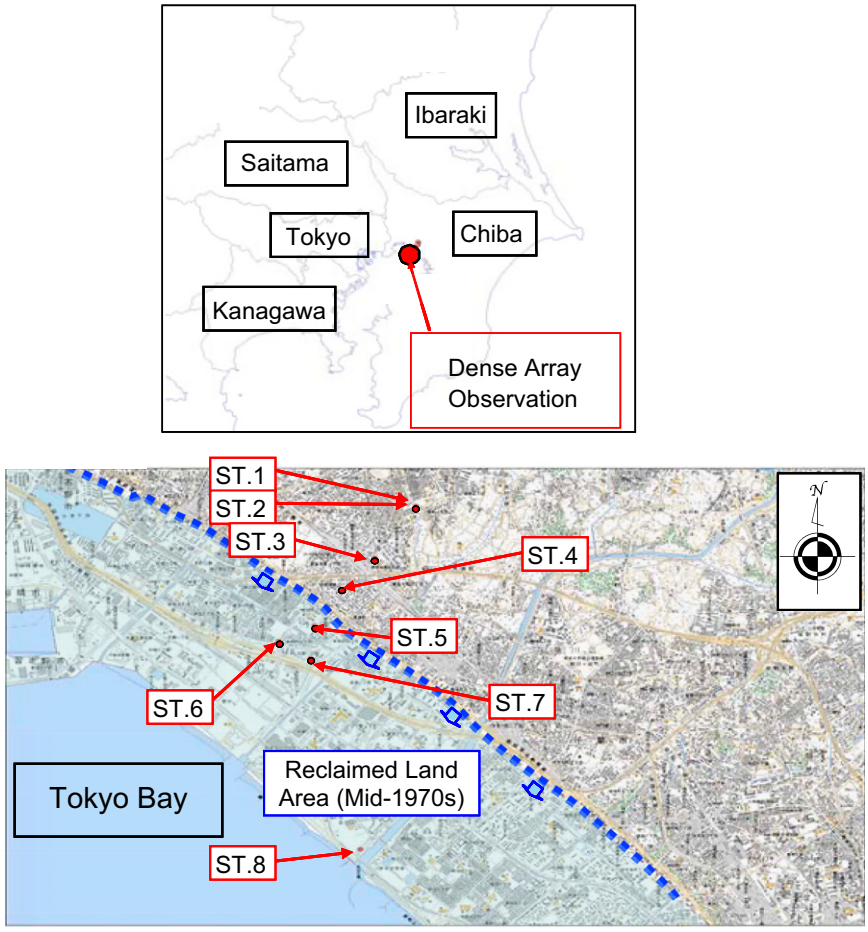

Fig. 13. Locations of the sensors of the dense array observation system at Narashino, Chiba (Tokyo Bay area). (For interpretation of the references to color in this figure, the reader is referred to the web version of this article.)

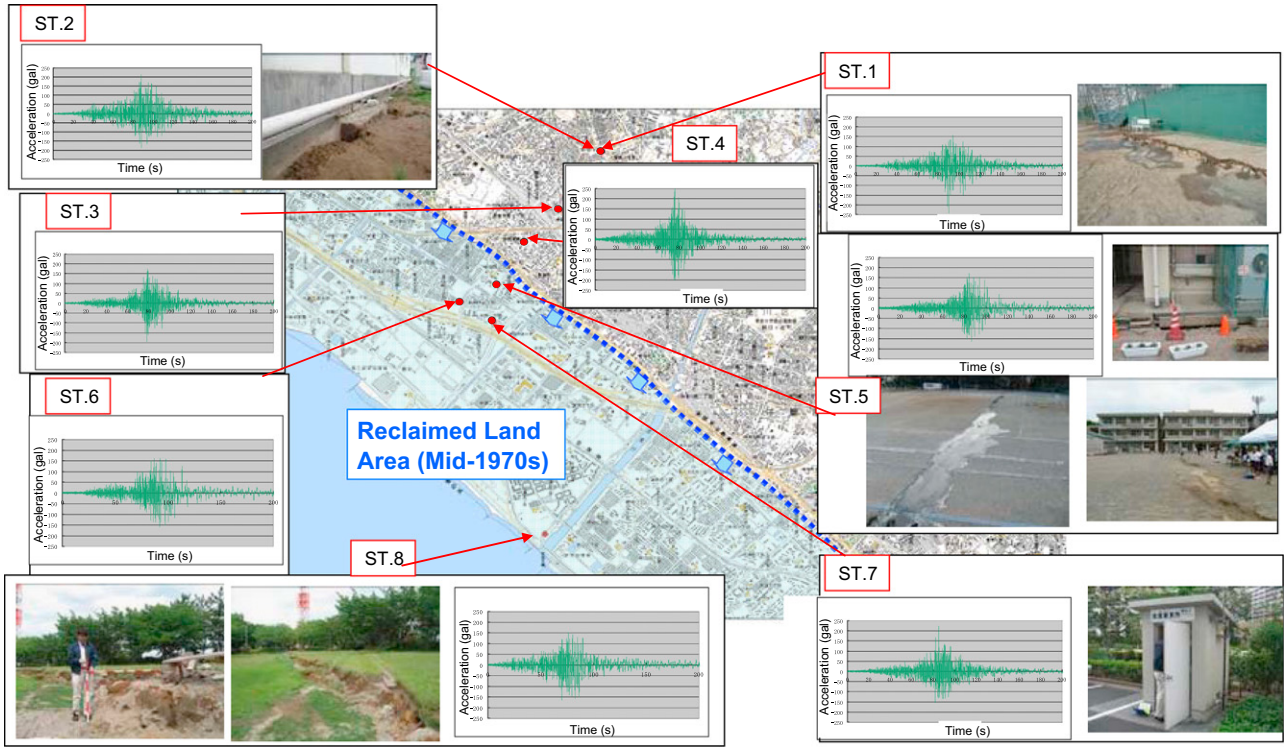

Fig. 14. Observed acceleration (EW component at GL. − 2 m) and damage around the stations of the dense array observation system at Narashino, Chiba.

around the stations, while no significant changes were found in the time histories observed in the inland area.

Fig. 15 compares the Fourier amplitudes of the acceleration observed in the reclaimed and the inland areas. The Fourier amplitudes are calculated for the blue-, red- and green-colored intervals. The intervals are roughly defined as those before the peak, after the peak and along with the surface wave. It is found that the time histories observed in the reclaimed area show a clear change in the predominant period from 0.8 to 1.5 s at the time of 80 s. On the other hand, no significant changes were found in the data observed in the inland area. The increase in the natural period to twice means that the stiffness of the ground decreased to about 1/4 of the original because of the effect of liquefaction.

3.4. Effect of cyclic loading by ground motion

In the foundation design, the soil liquefaction was evaluated using the F_L-value (Liquefaction Resistance Factor), as defined by Eq. (3) (JRA (Japan Road Association): Bridge Design Specifications (1996)). If the results of the F_L-value turn out to be less than 1.0, the layer is regarded as having the potential for liquefaction.

$$F_L = R/L \tag{3}$$

$$R = c_w R_L \tag{4}$$

where

F_L: Liquefaction resistance factor
R: Dynamic shear strength ratio
L: Seismic shear stress ratio
R_L: Cyclic triaxial shear stress ratio
c_W: Modification factor for earthquake ground motion

(For Type I earthquake ground motion)

$$c_w = 1.0 \tag{5}$$

(For Type II earthquake ground motion)

$$c_w = \begin{cases} 1.0 & (R_L \leqq 0.1) \\ 3.3R_L + 0.67 & (0.1 < R_L \leqq 0.4) \\ 2.0 & (0.4 < R_L) \end{cases} \tag{6}$$

Since cyclic triaxial shear stress ratio R_L changes significantly, according to the repeated property of seismic ground motions, the ratio is modified by Eqs. (5) and (6) depending on the Type I or Type II earthquake ground motions. Type I and Type II earthquakes correspond to an interplate earthquake with a large magnitude over 8.0 and an inland near-field type of earthquake with a magnitude around 7.0. Since the number of repeated Type II earthquakes is relatively smaller than

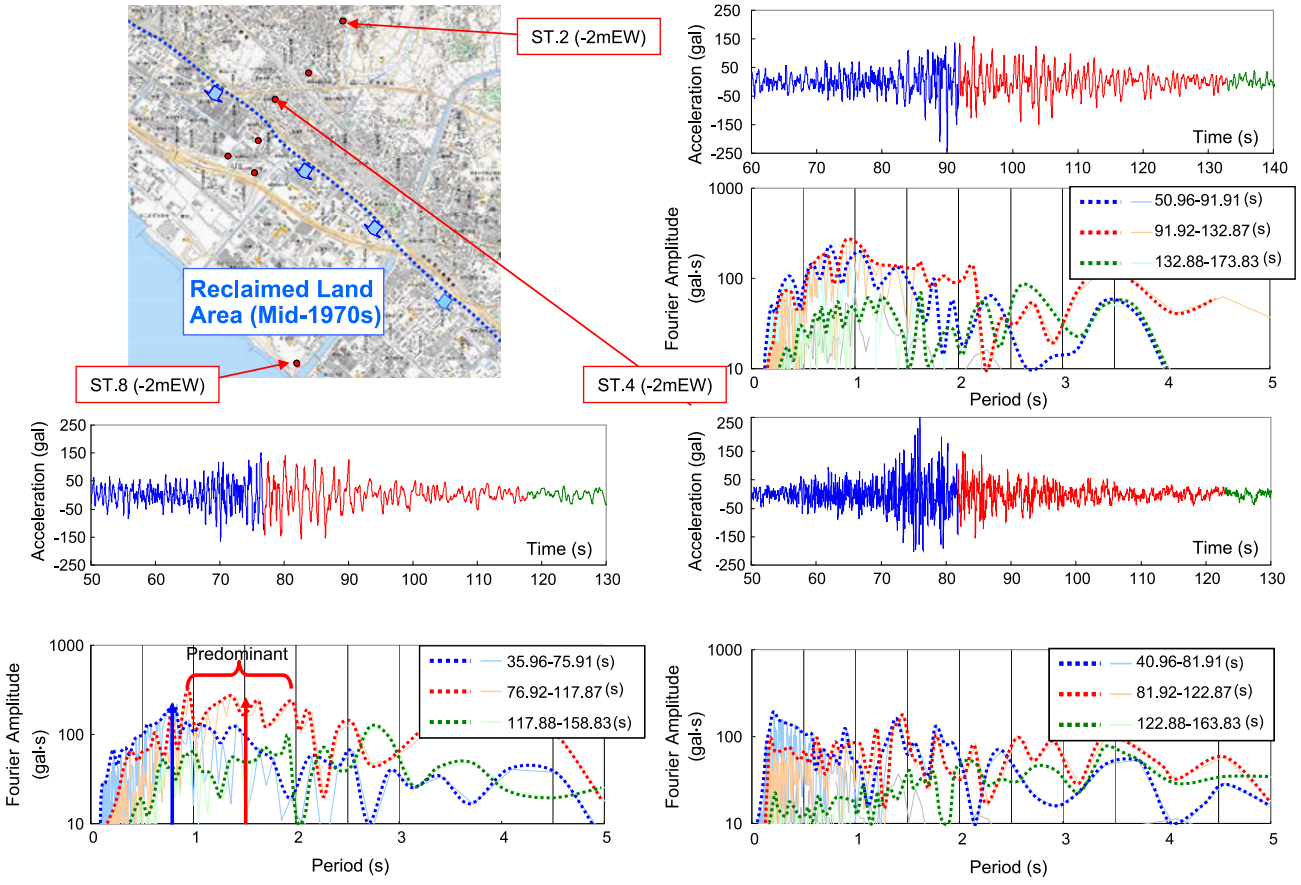

Fig. 15. Spectral analyses of the observed acceleration time histories. (For interpretation of the references to color in this figure, the reader is referred to the web version of this article.)

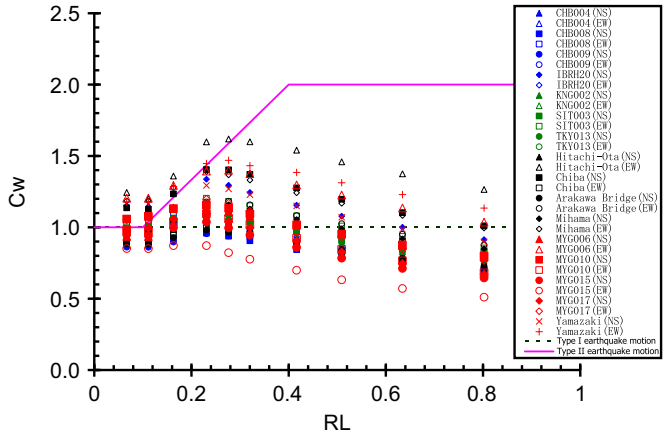

Fig. 16. Cyclic loading property of the earthquake ground motions of the 2011 off Pacific Coast of Tohoku Earthquake.

Type I earthquakes, c_w increases from 1.0 to 2.0 depending on R_L. The c_w obtained through the statistical analysis of 130 sets of records for past earthquakes, including six interplate-type earthquakes and two inland-type earthquakes (Azuma and Tamura, 1997). It should be noted here that R_L was obtained based on the results of laboratory undrained cyclic triaxial tests. To define the liquefaction, 20 cycles and 5% axial stain are used for the standard number of cyclic loadings and the strain. Therefore, when the cyclic number is less than 20, c_w increases to over 1.0. When the cyclic number is much larger than 20, the degree of liquefaction grows.

The repeated property of the ground motions obtained during the 2011 Great East Japan Earthquake was studied in comparison with that of past earthquakes. 32 sets of records obtained for the ground surface were used and the effect of the number of cyclic loadings and the duration time on the cyclic triaxial shear strength was analyzed using the accumulated damage theory.

Fig. 16 shows the analyzed c_w for the earthquake ground motions. The data dispersion is relatively large, but compared with past data, c_w is almost the same when R_L is less than about 0.4, while c_w decreases when R_L is larger than 0.4 with an increasing effect. In general, however, the liquefaction potential becomes smaller when R_L is larger than about 0.4.

4. Conclusion

This paper presents the strong motion observation data obtained for liquefied and non-liquefied grounds and raises preliminary discussions on the mechanism of soil liquefaction based on the strong motion observation data. The effect of the duration and the number of cyclic loadings of the strong motions on the progress of the soil liquefaction phenomenon was also studied by making a comparison with that recorded in past strong motion data.

The following preliminary results are summarized as

(1) Acceleration responses and excess pore water pressure records were observed for a levee in the Naruse River. The excess pore water pressure increased with the amplitude of acceleration and a dissipation of the pressure was clearly observed.

(2) At Narashino Station in Chiba, dense array observation data were obtained both for the reclaimed land and the inland areas. An elongation of the natural period was clearly recognized in the time histories with the progress of the soil liquefaction. On the reclaimed land, the soil liquefaction occurred at the peak acceleration of 200–250 gal and the period elongated about twice, which means the stiffness decreased to 1/4 of the original.

(3) Repeated property c_w of the ground motions was studied using the 32 sets of records observed in the 2011 Great East Japan Earthquake. The repeated property is similar to those of past interplate earthquakes. The duration is much longer than in past earthquakes, but the effect on the soil liquefaction strength was not remarkable. When liquefaction strength R_L is less than about 0.4, the effect is almost the same as in past earthquakes, but the effect is larger when strength R_L is larger than about 0.4.

Acknowledgments

This study was discussed in the "Committee to Study Countermeasures against Soil Liquefaction", which was established at MILT. The authors offer their sincere thanks to all the committee members for the fruitful discussions.

References

Azuma, T., Tamura, K., 1997. Evaluation method of soil resistance against liquefaction considering cyclic loading effect of earthquake ground motions. Civil Engineering Journal 39 (9), 50–55.

Creager, W.P., Justin, J.D., Hinds, J., 1945. Engineering for dams. Earth, Rock-fill, Steel and Timber Dams, vol. III. Wiley, New York, pp. 648–649.

JRA (Japan Road Association): Bridge Design Specifications, 1996. Part V. Seismic Design. JMA website: 〈http://www.jma.go.jp/jma/en/2011_Earthquake/Information_on_2011_Earthquake.html〉 (accessed 16.10.12).

Kataoka, S., Nagaya, K., Matsuoka, K., Kaneko, M., 2011. Strong Motion and Earthquake Response Records of the 2011 off the Pacific Coast of Tohoku Earthquake. In: Proceedings of the 43rd Joint Meeting of United-States–Japan Panel on Wind and Seismic Effects, UJNR, August 2011.

MLIT Committee to Study Countermeasures against Soil Liquefaction: 〈http://www.mlit.go.jp/report/press/kanbo08_hh_000154.html〉, 2011.

NIED, 2012 Website: 〈http://www.kyoshin.bosai.go.jp/〉. (accessed 16.10.12).

NILIM, 2012 Website: 〈http://www.nilim.go.jp/japanese/database/nwdb/index.htm〉. (accessed 16.10.12).

Yoshida, N., Towhata, I., 2003. YUSAYUSA-2 SIMMDL-2, Theory and Practice (Version 2.10). 〈http://www.civil.tohoku-gakuin.ac.jp/yoshida/computercodes/English_01.htm〉.

Yoshida, Y., Ueno, H., Muto, D., Aoki, S., 2011. Source process of the 2011 off the Pacific Coast of Tohoku earthquake with the combination of teleseismic and strong motion data. Earth Planets and Space 63, 565–569.